Mixed-conductive membrane composed of natural hematite and $Ni_{0.8}Co_{0.15}Al_{0.05}LiO_{2-\delta}$ for electrolyte layer-free fuel cell

Chen Xia, Muhammad Afzal, Baoyuan Wang, Aslan Soltaninazarlou, Wei Zhang, Yixiao Cai, Bin Zhu*

[1]*Department of Energy Technology, Royal Institute of Technology, Stockholm SE 10044, Sweden*
[2]*Hubei Collaborative Innovation Center for Advanced Organic Materials, Faculty of Physics and Electronic Technology, Hubei University, Wuhan, Hubei 430062, China*
[3]*Department of Engineering Sciences, Ångström Laboratory, Uppsala University, 751 21 Uppsala, Sweden*

*Corresponding author. Tel: (+46) 08-7907403; Email: binzhu@kth.se; zhubin@hubu.edu.cn

Abstract

Very recently, natural hematite has been developed as an electrolyte candidate for solid oxide fuel cells (SOFCs), because of its considerable ionic conductivity. In this work, to exploit more practical applications of natural hematite, we report a novel mixed-conductive composite made of natural hematite (α-Fe_2O_3) and semiconductor $Ni_{0.8}Co_{0.15}Al_{0.05}LiO_{2-\delta}$ (NCAL) to act as membrane layer in a new SOFC technology, electrolyte-layer free fuel cell (EFFC). The Hematite-NCAL composite was synthesized directly from natural hematite and commercial NCAL by solid-state blending and high-temperature calcination. The EFFC were constructed into a sandwich architecture with Hematite-NCAL as the membrane and NCAL pasted-Ni foams as the electrodes. Electrochemical impedance spectra (EIS) and direct current (DC) polarization measurements were carried out to investigate the electrical conductivity of the composite. A high ionic conductivity of 0.16 S cm^{-1} is achieved by the composite at 600 ºC with mass ratios of 7:3 (7Hematite: 3NCAL). When operated at low temperatures, the as-designed fuel cell demonstrated superior power densities of 554 mW cm^{-2} at 600 ºC and 342 mW cm^{-2} at 500 ºC. Considering the competitive cost, abundant resource and eco-friendliness of natural hematite, our findings indicate the Hematite-NCAL can be a highly promising candidate for advanced low-temperature SOFC applications. Copyright © 2016 VBRI Press.

Keywords: Electrolyte layer-free fuel cell, mixed-conductor, membrane, natural hematite, $Ni_{0.8}Co_{0.15}Al_{0.05}LiO_{2-\delta}$.

Introduction

In the past few decades, solid oxide fuel cells (SOFCs) have been a research focus in solid state ionic and material science due to their tremendous potential in energy conversion applications. SOFCs have attracted much interest because of their superiorities of high energy conversion efficiency, fuel flexibility and minimal pollution emissions [1-4]. Nevertheless, the typical operating temperature of SOFCs is as high as 800–1000 ºC, resulting in serious issues such as high manufacturing costs, long start-up step [5] as well as unacceptably fast performance degradation rates [6] of the devices, which impedes the practical application and commercialization of SOFCs. In this regard, it is fairly important to explore new alternate materials with desirable ionic conductivity and advanced technologies for developing low-temperature (400-600 ºC) SOFCs [7, 8].

Recent reports have raised natural minerals as a highly promising research topic in energy conversion field [9, 10]. For example, natural minerals of the tetrahedrite

($Cu_{12-x}M_xSb_4S_{13}$) and tennantite ($Cu_{12-x}M_xAs_4S_{13}$) [11] have been utilized as a direct source of thermoelectric materials for power generation. In previous study, a widespread natural ore of hematite (α-Fe_2O_3) [10] on earth showed enormous development potentials in solid state ionic filed, especially in the SOFC application. The natural hematite-based fuel cell reached an inspiring power output of 467 mW cm^{-2} at 600 ºC. Our latest study further modified this natural hematite through nanocomposite approach, the resultant mineral-based composite exhibited an ionic conductivity as high as 0.116 S cm^{-1} at 600 ºC with an activation energy of 0.50 eV (400-600 ºC) [12]. These preliminary achievements have proved that the use of natural minerals can be an underlying route to develop low-temperature SOFCs. Meanwhile, a new advanced SOFC technique, electrolyte layer-free fuel cell (EFFC) [13, 14], was proposed and explored intensively in recent years. The design concept of EFFC is deemed to be another potential effective route for for developing low-temperature SOFCs, as its operational temperature ranges from 300 to 600 ºC [15]. Typically, the core membrane layer of EFFC device is a

homomorphous material constituted by an ionic conductor and a semiconductor with efficient catalytic activity for both anodic and cathodic reactions, e.g., samarium-doped CeO_2 (SDC)-$Li_{0.15}Ni_{0.45}Zn_{0.4}O_x$ composite and samarium-doped CeO_2/Na_2CO_3 (NSDC)-$Sr_2Fe_{1.5}Mo_{0.5}O_{3-\delta}$ composite [**16**]. Several working principles such as nano-redox, n-p bulk-heterojunction and Schottky junction [**17**] have been proposed to study EFFC by Zhu et al from various perspectives. EFFC is a genuine low-temperature operational device, as shown in a notable example, gadolinium-doped CeO_2 (GDC)-$LiNiO_2$ EFFC has reached a peak power output of 400 mW cm^{-2} at 500 ºC [**18**]. At present, exploring new multi-function composites is one of the main research activities for such devices.

In this study, we combine the aforementioned two routes to design a new EFFC device based on a mixed-conductive composite membrane made of natural hematite and semiconductor material $Ni_{0.8}Co_{0.15}Al_{0.05}LiO_{2-\delta}$ (NCAL). The membrane is fabricated via a simple and feasible process with materials sourced from robust natural hematite and commercial NCAL powder. The as-designed cell device is assembled in a symmetrical configuration with NCAL slurry pasted Ni foam on both sides of the membrane layer as electrodes. The phase structure, morphology and electrical property of the as-prepared Hematite-NCAL composite are investigated. The EFFC device is operated with H_2 as fuel and evaluated in a low temperature region (500 ºC to 600 ºC).
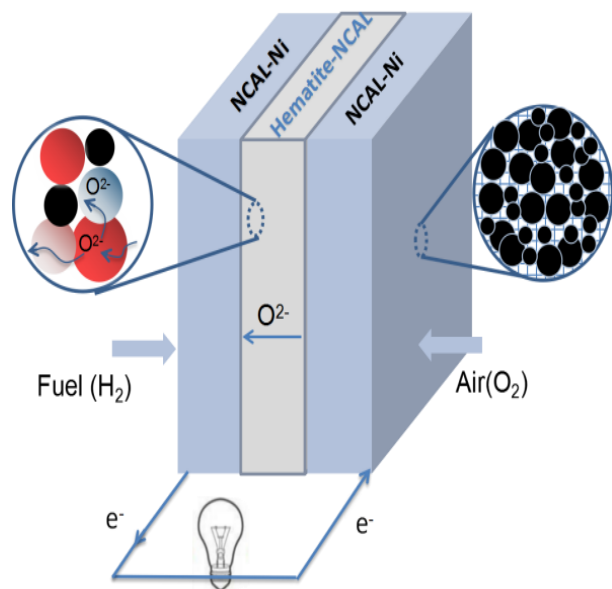

Fig. 1. Schematic diagram for the architecture of the fuel cell device.

Experimental

Material and preparation

The natural hematite utilized in this study is a high-grade ore exploited in Laiwu area in the northeastern China, with an exploration reservation in excess of 500 million tons. It belongs to skarn type iron deposit [**10**], comprising of hematite (α-Fe_2O_3 68.359 wt.%), quartz (SiO_2 19.039 wt.%,) and some other impurities. The

semiconductor material NCAL was purchased from Tianjin Bamo Sci. & Tech. Joint Stock Ltd, China.

Hematite-NCAL composite was prepared through a direct solid-state blending method and followed by a high temperature calcination process. Raw hematite and commercial NCAL powders were mixed with various weight ratios of 5:5, 6:4, 7:3 and 8:2 in an agate mortar respectively and ground thoroughly with modest amounts of ethanol to obtain a kermesinus mixture. The resultant mixture was dried at 300 ºC for 0.5 h and then calcined at 1000 ºC in air for 4 h. Subsequently, the resulting mixture was ground again completely to get the final powder product, Hematite-NCAL composite. In parallel, NCAL-Ni electrode was fabricated using NCAL slurry and nickel foam (Ni-foam). Firstly, the NCAL was processed into a slurry form by mixing its commercial powder with glycerol in ethanol (10% volume ratio of ethonal) and ground completely. Thereafter, the resultant slurry was pasted evenly on Ni-foam and desiccated at 300 ºC to obtain the NCAL-pasted Ni-foam (NCAL-Ni).

Fuel cell construction

Hematite-NCAL composite powder as the membrane layer was sandwiched between two NCAL-Ni layers to form a symmetric configuration of *NCAL-Ni | Hematite-NCAL | NCAL-Ni*. The powder and electrodes were compacted uniaxially into pellet under a pressure of 250 MPa. The resultant pellet is 13 mm in diameter and 2.0 mm in thickness. The schematic diagram of the designed fuel cell device is shown in **Fig. 1**.

Characterizations

Phase analysis of the samples were carried out by a Bruker D8 advanced X-ray diffractometer (Germany, Bruker Corporation) with Cu Kα radiation (λ=1.54060 Å) as the source operating at 45 kV. Particle morphologies and microstructures of the samples were investigated by JSM7100F field emission scanning electron microscope (FESEM, Japan) equipped with energy dispersive spectrometer (EDS) operating at 15kV.

Electrochemical measurements

Electrical properties of the sample and electrochemical properties of the device were studied with electrochemical impedance spectra (EIS) test at 400~600 ºC in H_2/air atmosphere, using an electrochemical work station (CHI660B, Cheng Hua Corp.). Samples for EIS measurements were fabricated as a symmetrical configuration as *Ag paste | sample | Ag paste*. The applied frequency range was from 0.01 Hz to 1M Hz, and the signal amplitude was 10 mV. Electronic conductivity of the sample was measured by direct current (DC) polarization method using a Hebb-Wagner ion blocking cell, in a configuration of *Pt (foil) | sample | Pt (foil)*. The measurement was performed on a digital micro-ohm meter (KD2531, Kangda Electrical Co., Ltd.).

The fuel cells were operated and measured using a computerized instrument (ITECH IT8511, Jiangsu, China) in a temperature range of 500~600 ºC under atmospheric pressure. Hydrogen and air were supplied as fuel and oxidant at a flow rate of 80-120 ml min-1. The

cell voltage and current were collected under the programmable electronic load.
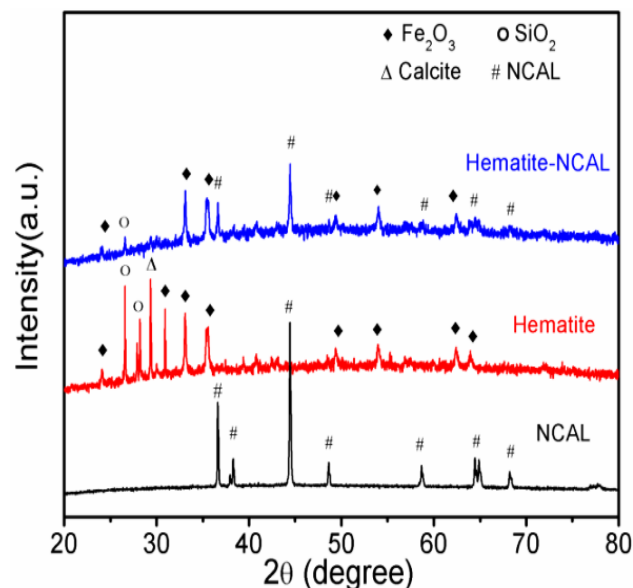
Fig. 2. XRD patterns of raw hematite, commercial NCAL and the prepared Hematite-NCAL composite.

Results and discussion

Structural and morphological study

Fig. 2 depicts the XRD patterns of raw hematite, commercial NCAL, and the synthesized Hematite-NCAL composite. The pattern of hematite (LW) is identified to Fe_2O_3 (JCPDS 79-1741), SiO_2 (JCPDS 83-2465) and calcite ($CaCO_3$, JCPDS 83-0578), indicating the heterogeneity of this raw mineral material. The pattern of NCAL shows sharp diffraction peaks, reflecting the good crystallinity of NCAL particles. For the Hematite-NCAL composite, the XRD pattern presents nearly all the characteristic diffractive peaks originate from hematite and NCAL, and no other phase appears, which indicates that the Hematite-NCAL composite is a heterogeneous material consisting of Fe_2O_3, NCAL and SiO_2 while there is no obvious chemical interaction among them. Significantly, the Δ peak of $CaCO_3$ from hematite cannot be detected in the XRD of Hematite-NCAL composite. That should be owing to the gradual decomposition of $CaCO_3$ during high temperature calcination process.

Fig. 3a shows the SEM micrograph of the raw material of natural hematite. It shows nano-sized particles in irregular shapes (50-200 nm), some bulks and agglomerations, due to the use of raw natural mined material. **Fig. 3b** presents the particle morphology of NCAL, in which the NCAL particles distribute uniformly, and the particle size ranges from a few hundred nanometers to nearly one micron. Despite the uneven and loose distribution of raw hematite particles, after blending and sintering processes, more uniformly distributed and closely contacted particles are observed in the final products of Hematite-NCAL composite (**Fig. 3c**). The composite basically consists of nano-sized grains and a small fraction of aggregations (~ 1 μm). Generally,

membrane layer with uniform, compact and small particles are more likely to offer sufficient active sites for electrochemical reactions [**19**].
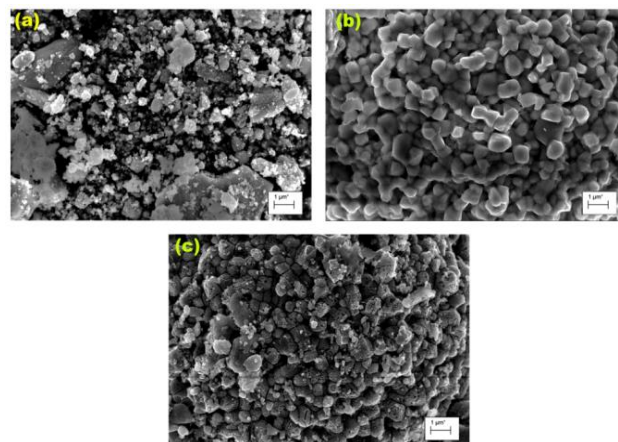
Fig. 3. SEM images of (a) raw hematite, (b) commercial NCAL and (c) the prepared Hematite-NCAL composite.

Fig. 4 presents EDS and elemental mapping results of the synthesized Hematite-NCAL composite. The EDS results reveal the presence of Fe, Si, Ni, Co, Al and O in the composite. It is evident that all major elements originated from Fe_2O_3, SiO_2, and NCAL are detected and exhibit pretty homogeneous distributions. The mapping results confirm the homogeneous distribution of hematite and NCAL in the composite.
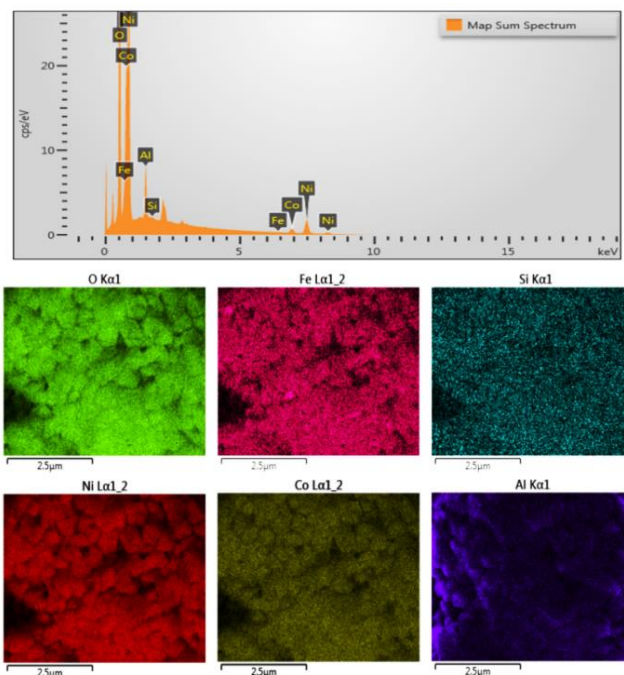
Fig. 4. EDS and elemental mapping of the prepared Hematite-NCAL composite.

Electrochemical properties

The EIS results of the fuel cells with 6Hematite-4NCAL, 7Hematite-3NCAL and 8Hematite-2NCAL are shown in **Fig. 5**. The measurements were performed in H_2/air atmosphere at 550 ºC and 600 ºC . Generally, the high-

frequency intercepts on the real axis are mainly result from the cell ohmic resistances (R_o), while the arcs of the EIS curves represent the electrode polarization resistances (R_p) of the cell [20], as indicated in **Fig. 5**. As can be observed, the three cells reveal a small intercept on the real axis of the semicircle at 600 ºC, which implies that the electrode reactions are kinetically fast [21], and proves that the three composites have high catalytic activity for both H_2 and O_2.
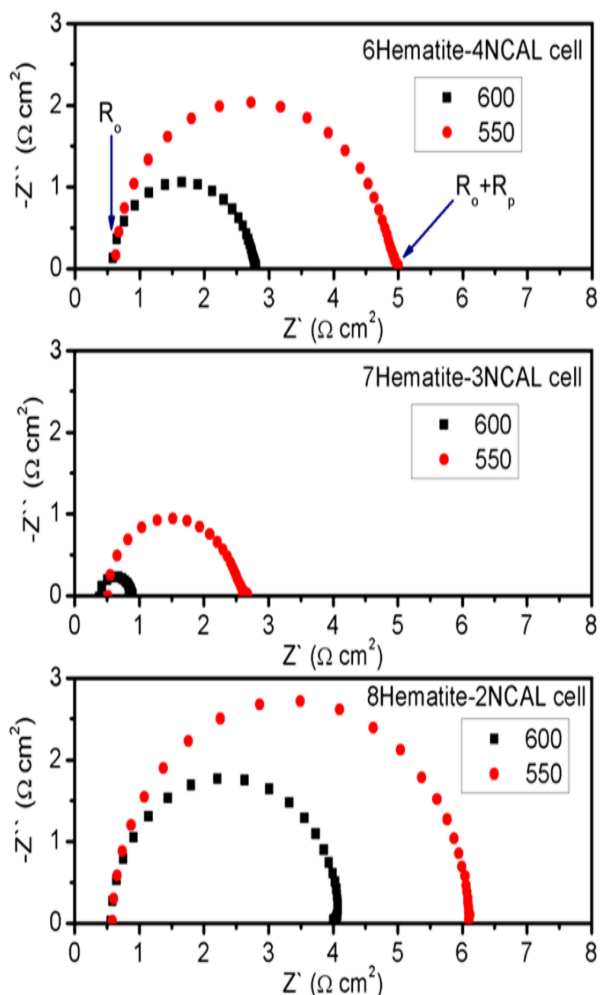

Fig. 5. Impedance spectra of fuel cells with 6Hematite-4NCAL, 7Hematite-3NCAL and 8Hematite-2NCAL tested in H_2/air atmosphere at 550 ºC and 600 ºC.

The comparison among the EIS results for different cells indicates that the R_o of the 7Hematite-3NCAL cell is slightly lower than those of other two cells at both 550 ºC and 600 ºC. However, the R_p of the three cells show significant difference. The 7Hematite-3NCAL cell has a much lower R_p (2.1 Ω cm^2 at 550 ºC and 0.5 Ω cm^2 at 600 ºC) than 6Hematite-4NCAL cell (3.9 Ω cm^2 at 550 ºC and 2.3 Ω cm^2 at 600 ºC) and 8Hematite-2NCAL cell (5.0 Ω cm^2 at 550 ºC and 3.5 Ω cm^2 at 600 ºC). The result manifests that the 7Hematite-3NCAL sample possesses the best catalytic activity for electrode electrochemical reaction among these composites.

To further characterize the material electrical properties, the EIS measurements of a device *Ag paste / 7Hematite-3NCAL / Ag paste* were conducted. **Fig. 6a**

displays the EIS results acquired in H_2/air atmosphere from 400 ºC to 600 ºC. An equivalent circuit mode of R_o/R_1(CPE$_1$)/R_2(CPE$_2$) was used to fit the original data, the fitting result (solid line) at each temperature share a same feature, squashed semicircle. It is well known that the intersection of semicircle in the high frequency region and the associated real axis value corresponds to the ohmic resistance (R_o) of the sample [14, 22], which is contributed by both the oxygen ions and electrons. Moreover, another intersection of the semicircle in the low frequency region with real axis corresponds to grain boundary resistance, which decreases noticeably with elevated temperatures from 400 ºC to 600 ºC.
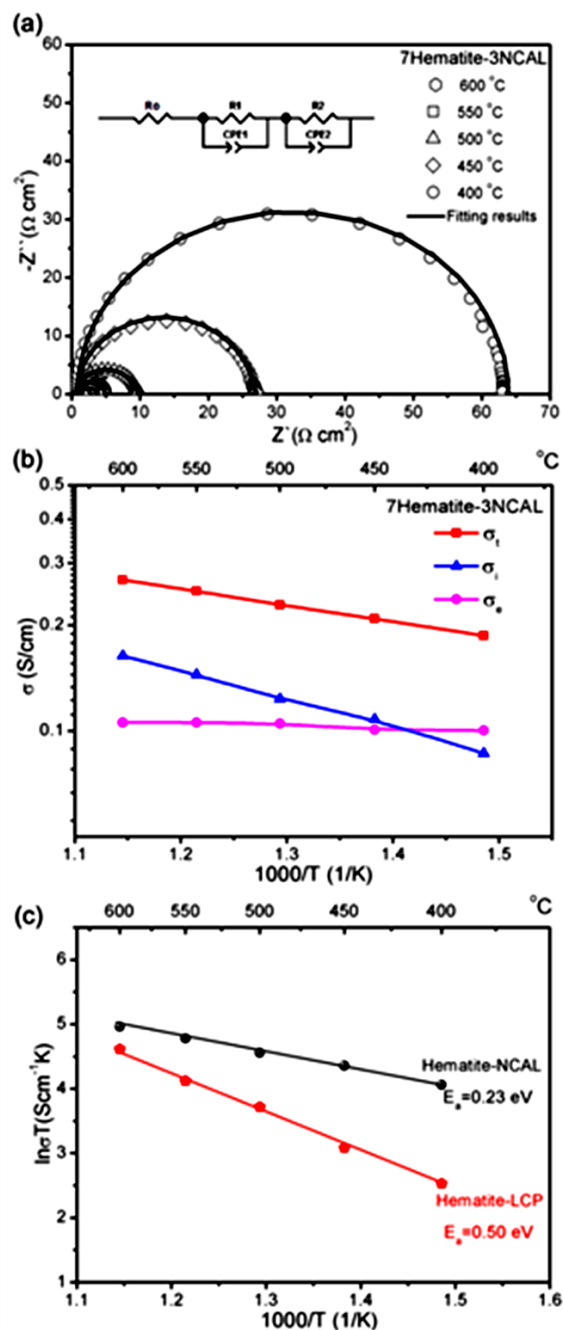

Fig. 6. (a) EIS results of device *Ag paste / 7Hematite-3NCAL / Ag paste* acquired in H_2/air from 400 ºC to 600 ºC. (b) Electrical conductivity results of the 7Hematite-3NCAL composite; (b) Comparison of ionic conductivity and activation energy of the 7Hematite-3NCAL composite with former mineral based oxide-ion conductors.

The electrical conductivity of 7Hematite-3NCAL composite consists of both electronic and ionic contributions. Consequently, the total electrical conductivity (σ_t) of the composite at various temperatures can be obtained according to the equation:

$$\sigma_t = L/(R_o \times S)$$

in which L is the pellet thickness and S denotes the effective area. Besides, in order to identify the conductivity contributed exclusively by electrons, Hebb-Wagner ion-blocking cell in a configuration of *Pt (foil) / 7Hematite-3NCAL / Pt (foil)* was used to measure the electronic conductivity (σ_e) of the composite. By this means, the ionic conductivity (σ_i) can also be estimated according to the equation: $\sigma_i = \sigma_t - \sigma_e$.
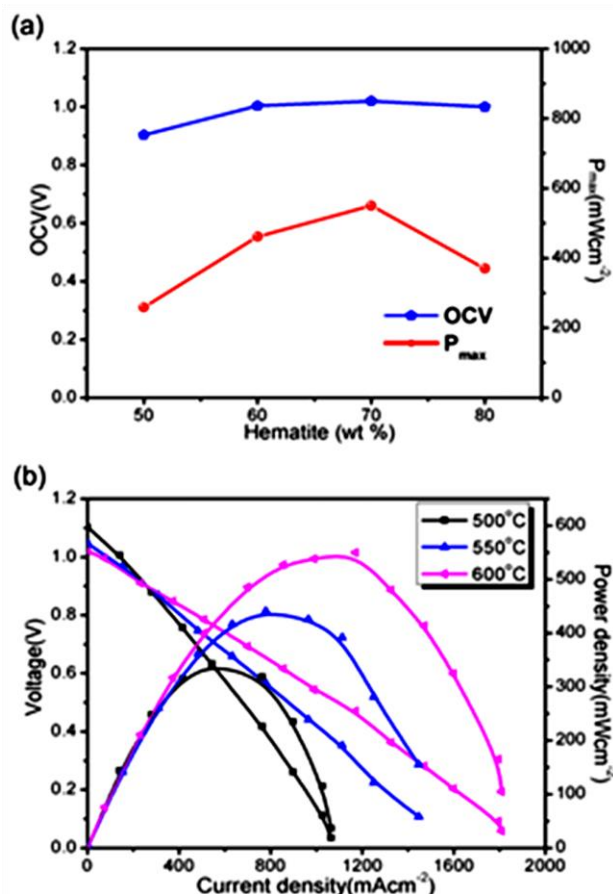
Fig. 7. (a) OCV and power density values for fuel cells based on Hematite-NCAL with different compositions. (b) Current density–voltage and power density characteristics for the fuel cells using 7Hematite-3NCAL at 500-600 ºC.

As illustrated in **Fig. 6b**, the measured σ_e increases from 0.100 S cm^{-1} to 0.106 S cm^{-1} as temperature elevates from 400 ºC to 600 ºC. The corresponding conductivity curve displays a negligible slope, which is similar to the electronic conducting behavior of NCAL [**23**]. As a result, the calculated σ_i starts from 0.08 S cm^{-1} at 400 ºC and reaches 0.16 S cm^{-1} at 600 ºC, which is much higher than the previously reported conductivity of hematite (LW) [**10**]. This suggests that an excellent ionic conductivity has been realized in our mixed-conductive composite by

intermingling natural hematite and semiconductor in a proper content ratio and treatment. The extraordinary ionic conductivity is possibly benefit from the interfacial conduction effect [**24**] at the interface regions formed among heterophasic nanoparticles.

Fig. 6c shows the ionic conductivities of the 7Hematite-3NCAL composite corresponding to Arrhenius plots at various temperatures. For better comparison, we also plotted previously reported result of Hematite-LaCePrO$_x$ (Hematite-LCP) composite [**12**] in Fig. 6c. It can be found that our 7Hematite-3NCAL sample exhibits a higher ionic conductivity in the temperature range of 400-600 ºC. Additionally, the activation energy of the sample can be calculated according to the Arrhenius equation:

$$\sigma T = A\exp\left[- E_a/(kT)\right]$$

where T is the absolute temperature, A is the pre-exponential factor, Ea is the activation energy, and k represents the Boltzmann constant [**25**]. From **Fig. 6c,** the E$_a$ of the 7Hematite-3NCAL composite was calculated to be an exceptional low value of 0.23 eV, which is significantly lower than that of pure Hematite-LCP (0.50 eV). The similar phenomenon of low activation energy can be also observed in other mixed-conductive systems. For instance, the values of activation energy for oxygen migration is 0.65 eV in the nanoscaffold SDC-SrTiO$_3$ [**26**] and 0.4 eV in GDC/KAZ-LiNiCuZnO$_x$ at 400-600 ºC [**27**]. This may be caused by such interfacial behavior due to the semiconductor/ionic conductor heterostructure in the composite.

Fuel cell performances

Fig. 7a shows the electrochemical performances for the four *NCAL-Ni / Hematite-NCAL / NCAL-Ni* cells with different ratios of Hematite-NCAL at 600 ºC. From the figure, it is clear to see that the cells with nonnegligible amount of electronic conductor does not show any open circuit voltage (OCV) losses. All of the cells exhibit OCVs with values over 0.9 V, especially, when the weight ratio of hematite is more than 60 wt.%, the cells display much higher OCVs of around 1.0 V. It is interesting to find that the fuel cell devices have no any short circuit issue even though we used mixed-conductive material as the membrane layer. This is primarily ascribed to the anodic Schottky junction effect in our sandwich-structured EFFC device. As reported [**17**], providing H$_2$ into the device will generate a thin metal layer originated from reducing the semiconducting NCAL electrode on the anode side. In the meantime, a Schottky barrier is established at the metal-semiconductor interface to prevent electron from transporting through the internal structure of cell [**28**]. It was also reported that the barrier field may provide the secondary driving force for ionic transport in addition to the chemical potential. Thereby, the mixed conductor membrane can realize the electrolyte purpose without causing any short-circuit issue. The peak power densities of the four cells are 260 mW/cm^2, 460 mW/cm^2, 554 mW/cm^2, and 370 mW/cm^2 at 600 ºC, respectively. Obviously, these cells present higher OCVs

and better output performances than that of pure hematite electrolyte fuel cells [**10**].

Meanwhile, significant correlation between the cell power outputs and different compositions of the composite is observed. As can be seen, the fuel cell based on 7Hematite-3NCAL membrane achieves the highest peak power density of 554 mW/cm^2, which is distinctly superior to those of other three cells. This is in accordance with the EIS results in **Fig. 5**. When the hematite content was less than 70 wt% in the composite, the excessive NCAL caused the electron transport process to dominate, which causes a partial short circuit of the cell, leading to a decrease of OCV from 1.02 V to 0.91 V. When the hematite content was more than 70 wt% in the composite, the NCAL was insufficient to have significant interaction with hematite to improve the ionic conduction, thus resulting in a lower power density than that of 7Hematite-3NCAL. Therefore, integration of 70 wt.% hematite and 30 wt.% NCAL is the optimum composition for our composite to reach the best catalytic activity and fuel cell performance. Ulteriorly, the fuel cell with 7Hematite-3NCAL was operated at lower temperatures. As shown in **Fig. 7b**, a superior power density of 440 mW cm^{-2} has been achieved at 550 °C. At 500 °C, the fuel cell still delivers a superior power output of 342 mW/cm^2. This is a technically useful advancement with great commercialization potential. The results confirm the availability of low-temperature operation for Hematite-NCAL fuel cells. Compared with previous studies of hematite based fuel cells, ceria based fuel cells, and other mixed-conductive membrane fuel cells, our study demonstrates better performances at low temperature range of 500-600 °C, as listed in **Table 1**.

Table 1. Performance comparison of Hematite-NCAL membrane fuel cell with previously reported literature.

Membrane materials	Performances (500~600 °C)	OCVs (500~600 °C)	Reference
Hematite-NCAL	342~554 mW/cm^2	0.91~1.1 V	This work
Pure hematite	150~225 mW/cm^2	0.89~0.94 V	[10]
Hematite-LSCF	240~467 mW/cm^2	0.89~1.0 V	[10]
SDC	130~360 mW/cm^2	0.74~0.80 V	[29]
GDC-LiNiO$_2$	292~460 mW/cm^2	1.03~1.06 V	[18]
SCDC-NCAL (550 °C)	617 mW/cm^2	1.06 V	[30]
SDC-LNCS (550 °C)	312 mW/cm^2	0.94 V	[31]
SCD (Ca$_{0.04}$Ce$_{0.96-x}$Sm$_x$O$_{2-\delta}$)	LNCS (Li$_{0.3}$Ni$_{0.6}$Cu$_{0.07}$Sr$_{0.03}$O$_{2-\delta}$)		

As summarized in **Table 1**, it is clear to find that EFFCs based on mixed-conductive composite membranes made of natural hematite exhibit much higher outputs and OCVs than both pure SDC and hematite electrolyte SOFCs. A vertical comparison among the studies of hematite materials reflects that, from pure hematite to Hematite-LSCF and then to Hematite-NCAL, the corresponding fuel cells achieve evidently improved power outputs and OCVs. The Hematite-NCAL fuel cell even demonstrates a two-fold power density as that of hematite electrolyte fuel cell at 600 °C. When compared with doped ceria-semiconductor system, the proposed Hematite-NCAL composite shows comparable or even better fuel cell performances. Considering the merits of

natural hematite, such as ultra-low cost and zero-pollution, the proposed composite is proved to be a cost-effective and promising material for low-temperature SOFCs.

The advancements of current work can be attributed to the mixed-conductive property and heterophasic structure of the composite as well as the advantages of EFFC technology. As reported [**10, 12, 32**], both hematite (LW) and NCAL are good ionic conductors. The study of hematite (LW) has demystified that the Fe$_2$O$_3$ in the material can be easily reduced to oxygen-deficient Fe$_2$O$_{3-\delta}$ and form oxygen vacancies in H$_2$ atmosphere, and reoxidized to Fe$_2$O$_3$ under air circumstance to complete the full Fe^{3+} to Fe^{2+} redox cycle. This leads to a considerable ionic conductivity of hematite (LW) under fuel cell operational atmosphere. NCAL, as a typical example of lithiated transition metal oxides with unique layered structure has been reported with triple (H$^+$/O^{2-}/e$^-$) conducting properties and good oxygen reduction reaction (ORR) activity at low temperatures. It was reported that the high mobility of Li$^+$ in NCAL can promote O^{2-} and H$^+$ mobility as well, due to interaction in a dynamic situation. [**23**]. Besides, well-coupled ionic and electronic conductivities has been obtained in our Hematite-NCAL composite, as shown above, the tested electronic conductivity is on the same order of magnitude with the estimated ionic conductivity at 400-600 °C. This is quite significant to the fuel cell performance. Because benefiting from sufficient electronic and ionic conduction of Hematite-NCAL, the triple phase boundary (TPB) of both anode and cathode functional regions of the fuel cell device can be significantly extended, and the electrode polarizations are decreased accordingly [**33**]. This can be testified by **Fig. 5.**

Moreover, the heterophasic structure of the composite should also be emphasized. As reported [**23, 34**], the ionic conduction can be significantly enhanced by introducing semiconducting phase to ionic conductor. For instance, mixed-conductive composite Ca$_{0.04}$Ce$_{0.96-x}$Sm$_x$O$_{2-\delta}$-La$_{0.6}$Sr$_{0.4}$Co$_{0.2}$Fe$_{0.8}$O$_{3-\delta}$ (SCDC-LSCF) [**35**] achieved unexpectedly high ionic conductivity (0.188 S cm^{-1} at 600 °C) by mixing ionic conductor SCDC with semiconductor LSCF, demonstrating four times higher ionic conductivity than that of pure SCDC. Semiconductor/ionic conductor interfacial effect was proposed to explain this improvement. Due to such heterophasic interfacial effect, extra O aggregate in the semiconductor/ionic conductor interface region lead to a decreasing stoichiometry of oxygen in grain interior, which will cause the improvement of oxygen vacancies concentrations. The depletion of oxygen vacancies inside the SCDC-LSCF grain boundaries was observed to be significantly mitigated, resulting in an remarkable enhancement of ionic conductivity [**35, 36**]. In nanocrystalline composite especially, the interfacial effect is dominant in overall ionic transport [**37**], which is completely different from the ionic conduction mechanism in single phase material. This phenomenon was also reported in hematite/LaCePrO$_x$ system [**12**], which exhibited a far higher ionic conductivity than both pure hematite and LaCePrO$_x$, and in doped ceria-Li$_x$ZnO system [**34**], which showed superionic conductivity at very low temperature

range (>0.1 S cm^{-1} over 300 °C). In this study, the ionic conductivity of the hematite gets distinct enhancement and reaches up to 0.16 S cm^{-1} at 600 °C via an integration with NCAL. The material characterizations have indicated the heterophasic structure of the prepared Hematite-NCAL. Consequently, it can be speculated that the ionic conduction at heterophase interfaces is one of the primary reasons that leads to the high conductivity.

On the other hand, it is quite necessary to take into account the merits of EFFC device to explain the advancements of this work. Unlike the traditional SOFC structure, there is no anode/electrolyte/cathode 3 component structure in the conventional sense in EFFC devices. The only core component is the mixed-conductive layer, which plays a major role as the functional layer for both electrode catalytic reactions and ionic conduction. In traditional SOFC, the electrolyte/anode and electrolyte/cathode interfaces contribute to major polarization losses. However, such losses from interfaces can be avoided in EFFCs [**38**], which can be reflected by the small value of R$_p$ (0.5 Ω cm^2 at 600 °C) in this study (**Fig. 5**). More importantly, Hematite-NCAL composite as a mixed ionic and electronic conductor (MIEC) can never replace YSZ or SDC to be used as the electrolyte layer in traditional SOFC, since the shorting circuit problem will cause serious device OCV and power output losses. By feat of EFFC technology the superiorities of the mixed-conductive membrane can be better highlighted and brought into full play, such as, high ionic conduction and good catalytic activity. In another word, EFFCs create opportunities for Hematite-NCAL and many other promising mixed-conductive composite materials.

Conclusion

In summary, a novel mixed-conductive composite Hematite-NCAL based on natural mineral and semiconductor has been developed and applied as the membrane layer in EFFC. The characterization results prove that the prepared Hematite-NCAL is a heterogeneous nanocomposite and the constituents are distributed homogeneously. At the optimal composition, the ionic conductivity of the Hematite-NCAL composite can reach as high as 0.16 S cm^{-1} at 600 °C. Moreover, the composition of the composite remarkably influences the electrochemical performances of the cell. The cell with 7Hematite-3NCAL membrane exhibited a highest peak power output of 554 mW cm^{-2} at 600 °C. It also shows a promising low-temperature operation capacity, achieving sufficiently good performances of 343-440 mW cm^{-2} at 500-550 °C. Considering the merits of ultra-low cost and eco-friendliness, the proposed composite has been proved to be a high-efficient and cost-effective candidate for advanced EFFC technology. More profoundly, this work also provides a simple approach for extracting more potential of natural mineral-based SOFC and propel this technology ahead with commercialization possibility.
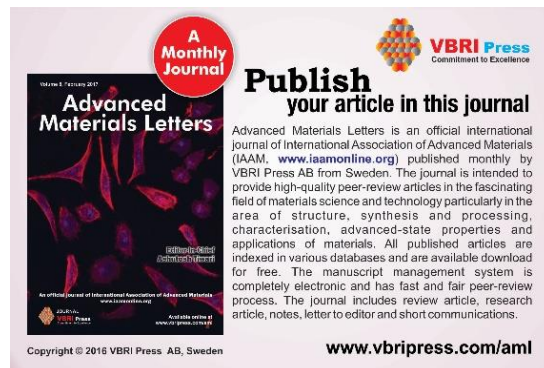
Author's contributions

Conceived the plan: CX, BZ; Performed the experiments: CX, MA, WZ, AS; Data analysis: CX, BW, YC; Wrote the paper: CX, BZ. Authors have no competing financial interests.

References

1. Singhal, S.C; *Solid State Ionics*, **2000**, *135*, 305. **DOI:** 10.1016/S0167-2738(00)00452-5
2. Ormerod, R.M; *Chem. Soc. Rev.,* **2003**, *32*, 17. **DOI:** 10.1039/B105764M
3. Park, S.; Vohs, J.M.; Gorte, R.J; *Nature*, **2000**, *404*, 265. **DOI:** 10.1038/35005040
4. Minh, N.Q; *Solid State Ionics*, **2004**, *174*, 271. **DOI:** 10.1016/j.ssi.2004.07.042
5. Huang, P.; Horky, A.; Petric, A; *J. Am. Ceram. Soc.*, **1999**, *82*, 2402. **DOI:** 10.1111/j.1151-2916.1999.tb02096.x
6. Wachsman, E.D.; Lee, K.T; *Science*, **2011**, *334*, 935. **DOI:** 10.1126/science.1204090
7. Singhal, S.C; *Solid State Ionics*, **2002**, *152*, 405. **DOI:** 10.1016/S0167-2738(02)00349-1
8. Leon, C.; Santamaria, J.; Boukamp, B.A; *MRS Bull*, **2013**, *38*, 1056. **DOI:** 10.1557/mrs.2013.264
9. Lu, X.; Morelli, D.T; *Phys. Chem. Chem. Phys*., **2013**, *15*, 5762. **DOI:** 10.1039/C3CP50920F
10. Wu, Y.; Xia, C.; Zhang, W.; Yang, X.; Bao, Y.Z.; Li, J.J.; Zhu, B; *Adv. Funct. Mater.*, **2015**, *10*, 201503756. **DOI:** 10.1002/adfm.201503756
11. Lu, X.; Morelli, D.T.; Xia, Y.; Zhou, F.; Ozolins, V.; Chi, H.; and Uher, C; *Adv. Energy Mater.*, **2013**, *3*, 342. **DOI:** 10.1002/aenm.201200650
12. Xia, C.; Cai, Y.; Ma, Y.; Wang, B.; Zhang, W.; Karlsson, M.; Wu, Y.; Zhu, B; *ACS Appl. Mater. Interfaces*, **2016**, *8*, 20748. **DOI:** 10.1021/acsami.6b05694
13. Zhu, B.; Raza, R.; Abbas, G.; Singh, M; *Adv. Funct. Mater.*, **2011**, *21*, 2465. **DOI:** 10.1002/adfm.201002471
14. Xia, Y.; Liu, X.; Bai, Y.; Li, H.; Deng, X.; Niu, X.; Meng, J; *RSC Adv.*, **2012**, *2*, 3828. **DOI:** 10.1039/C2RA01213H
15. Fan, L.; Wang, C.; Chen, M.; Zhu, B; *J. Power Sources*, **2013**, *234*, 154. **DOI:** 10.1016/j.jpowsour.2013.01.138
16. Lu, Y.; Zhu, B.; Cai, Y.; Kim, J.S.; Wang, B.; Wang, J.; Li, J; *Frontiers in Energy Research*, **2016**, *4*: 17. **DOI:** 10.3389/fenrg.2016.00017
17. Zhu, B.; Lund, P.D.; Raza, R.; Ma, Y.; Fan, L.; Afzal, M.; and Huang, Q.A; *Adv. Energy Mater*. **2015**, *5*, 1401895. **DOI:** 10.1002/aenm.201401895
18. Zhu, B.; Ma, Y.; Wang, X.; Raza, R.; Qin, H.; and Fan, L; *Electrochem. Commun.*, **2011**, *13*, 225. **DOI:** 10.1016/j.elecom.2010.12.019
19. Han, Y.; Lu, Y; *Comps. Sci. Technol.,* **2009**, *69,* 1231. **DOI:** 10.1016/j.compscitech.2009.02.028
20. Dusastre, V.; Kilner, J.A; *Solid State Ionics*, **1999**, *126*, 163 . **DOI:** 10.1016/j.compscitech.2009.02.028
21. Zhu, B.; Raza, R.; Qin, H.Y.; Liu, Q.H.; Fan, L.D; *Energy Environ. Sci.*, **2011**, *4*, 2986. **DOI:** 10.1039/C1EE01202A
22. Hu, H.; Lin, Q.; Zhu, Z.; Zhu, B.; Liu, X; *J. Power Sources*, **2014**, *248*, 577. **DOI:** 10.1016/j.jpowsour.2013.09.095
23. Xia, C.; Wang, B.; Ma, Y.; Cai, Y.; Afzal, M.; Liu, Y.; He, Y.; Zhang, W.; Dong, W.; Li, J.; Zhu, B; *J. Power Sources*, **2016**, *307*, 270. **DOI:** 10.1016/j.jpowsour.2015.12.086
24. Maier, J; *J. Electrochem. Soc.,* **1987**, *134*, 1524. **DOI:** 10.1149/1.2100703
25. Gu, H.; Chen, H.; Gao, L.; Zheng, Y.; Zhu, X.; Guo, L; *Int. J. Hydrogen Energy*, **2008**, *33*, 4681. **DOI:** 10.1016/j.ijhydene.2008.06.025

26. Yang, S. M.; Lee, S.; Jian, J.; Zhang, W. R.; Lu, P.; Jia, Q.X.; Wang, H. Y.; Noh, T. W.; Kalinin, S. V.; MacManus-Driscoll, J. L; *Nat. Commun.*, **2015**, *6*, 8588.
DOI: 10.1038/ncomms9588
27. Zhu, B.; Fan, L.; Zhao, Y.; Tan, W.; Xiong, D.; Wang, H; *RSC Adv.*, **2014**, *4*, 9920. **DOI:** 10.1039/C3RA47783E
28. Afzal, M.; Saleemi, M.; Wang, B.; Xia, C.; Zhang, W.; He, Y.; Jeevan, J.; Zhu, B; *J. Power Sources*, **2016**, *328*, 136.
DOI: 10.1016/j.jpowsour.2016.07.093
29. Yan, A.; Phongaksorn, M.; Nativel, D.; Croiset, E; *J. Power Sources*, **2012**, *210*, 374.
DOI: 10.1016/j.jpowsour.2011.10.081
30. Zhang, W.; Cai, Y.; Wang, B.; Deng, H.; Feng, C.; Dong, W.; Zhu, B; *Int. J. Hydrogen Energy*, **2016**, *41*, 18761.
DOI: 10.1016/j.ijhydene.2016.01.127
31. Hu, H.; Lin, Q.; Zhu, Z.; Liu, X.; Afzal, M.; He, Y.; Zhu, B; *J. Power Sources*, **2015**, *275*, 476.
DOI: 10.1016/j.jpowsour.2014.11.041
32. Fan, L.; Su, P. C; *J. Power Sources*, **2016**, *306*, 369.
DOI: 10.1016/j.jpowsour.2015.12.015
33. Dong, X.; Tian, L.; Li, J.; Zhao, Y.; Tian, Y.; Li, Y; *J. Power Sources*, **2014**, *249*, 270.
DOI: 10.1016/j.jpowsour.2013.10.045
34. Fan, L.; Ma, Y.; Wang, X.; Singh, M.; Zhu, B; *J. Mater. Chem. A*, **2014**, *2*, 5399. **DOI:** 10.1039/C3TA14098A
35. Wang, B.; Wang, Y.; Fan, L.; Cai, Y.; Xia, C.; Liu, Y.; Raza, R.; Aken, P.A.; Wang, H.; Zhu, B; *J. Mater. Chem. A*, **2016**.
DOI: 10.1039/C6TA05763B
36. Guo, X.; Maier, J; *J. Electrochem. Soc.*, **2001**, *148*, E121.
DOI: 10.1149/1.1348267
37. Sata, N.; Eberman, K.; Eberl, K.; Maier, J; *Nature*, **2000**, *408*, 946.
DOI: 10.1038/35050047
38. Lu, Y.; Zhu, B.; Cai, Y.; Kim, J. S.; Wang, B.; Wang, J.; Zhang, Y.; Li, J; *Front. Energy Res.*, **2012**, *4*, 17.
DOI: 10.3389/fenrg.2016.00017